ADVANCED MATERIALS INTERFACES
www.advmatinterfaces.de

Effects of Energy-Level Alignment on Operating Voltages of Blue Organic Light-Emitting Diodes

Tsubasa Sasaki, Taku Oono, Takahisa Shimizu, and Hirohiko Fukagawa**

Although organic light-emitting diodes (OLEDs) have been studied extensively for various applications, the effect of the electron behavior on the characteristics of OLEDs has rarely been discussed owing to the difficulty in investigating the actual energy levels. Understanding the correlation between energy levels and the characteristics of OLEDs is essential to improve the performances of blue OLEDs, since the materials with relatively large band gaps used in blue OLEDs make it difficult to deliver electrons from the cathode to the emitting layer (EML). Here, it is shown that the operating voltages of blue OLEDs strongly depend on the energy barrier between the cathode and the EML, which is clarified by investigating the energy-level alignment in blue OLEDs. It is found that a blue OLED fabricated using a superbase as the electron injection layer exhibits a lower operating voltage than conventional blue OLEDs fabricated using Li compounds. Moreover, there is a clear energy barrier between the cathode and the EML in conventional blue OLEDs, whereas there is no energy barrier in blue OLEDs fabricated using a superbase. Minimization of the energy barrier between the cathode and the EML is demonstrated to be essential to obtain blue emission at low operating voltages.

1. Introduction

Organic light-emitting diodes (OLEDs) have been extensively studied for several decades and have been commercialized in applications such as displays.[1–8] In order for OLED displays to become more vivid and energy efficient, the characteristics of red, green, and blue OLEDs must be improved. The characteristics of red and green OLEDs have reached maturity, whereas improving the characteristics of blue OLEDs includes some challenges, such as their high operating voltage, low efficiency, and short lifetime.[9–11] The reason for their high operating voltage is that the materials used in blue OLEDs have a large band gap, making it difficult to inject electrons and holes. In general, reactive materials such as alkali metals with work functions (WFs) lower than 3 eV are used at cathode/organic layer interfaces as the electron injection layer (EIL) to improve the electron injection properties of blue OLEDs, as in the case with red and green OLEDs.[12–14] In recent years, alkali metals have often been doped into the electron transport layer (ETL) in blue OLEDs, which is considered to be effective for improving electron injection/transport properties.[15–19] Although blue OLEDs with low operating voltages can be realized by using alkali-metal-doped ETLs/EILs, the detailed mechanism and a definitive strategy to lower the operating voltage of blue OLEDs are unclear. This is mainly because the correlation between the actual energy levels and the operating voltage of blue OLEDs has rarely been discussed. Since alkali metals such as Ba, Ca, and Cs are highly reactive, it has been difficult to investigate the electronic structure at organic/cathode interfaces when using alkali metals as a part of EILs and ETLs. In addition, little has been known until recently about the actual electron affinity (EA) of organic compounds with low EA, such as those used in blue OLEDs. By using low-energy inverse photoemission spectroscopy (LEIPS), Yoshida clarified that the actual EA is much lower than the EA estimated from the optical gap.[20,21] For past blue OLEDs, the EAs of the materials used as the emitting layer (EML) and ETL have been estimated to be ≈3 eV from the optical gap and ionization potential (IP), which is comparable to the WF of Li. However, the actual EA may be ≈1 eV smaller than the EA estimated from the optical gap, and it is important to discuss the effect of energy-level alignment on the operating voltage of blue OLEDs on the basis of the actual EA.

Here, we show that minimization of the energy barrier between the cathode and the EML is essential to obtain blue emission in OLEDs at low operating voltages, which is clarified by investigating the correlation between the operating voltage of blue OLEDs and the actual energy levels in blue OLEDs. We found that a blue OLED fabricated using the superbase 2,6-*bis*(1,3,4,6,7,8-tetrahydro-2H-pyrimido[1,2-a]pyrimidin-1-yl) pyridine (Py-hpp$_2$)[22,23] as the EIL, which can reduce the WF near the Al cathode to ≈2.0 eV, exhibited a lower operating voltage than blue OLEDs fabricated using Li compounds as the EIL and/or part of the ETL. It was also found by direct measurement of the EA using LEIPS that the EA of the emitting host in

T. Sasaki, T. Oono, T. Shimizu, H. Fukagawa
Japan Broadcasting Corporation (NHK)
Science & Technology Research Laboratories
1-10-11, Kinuta, Setagaya-ku, Tokyo 157–8510, Japan
E-mail: sasaki.t-he@nhk.or.jp; fukagawa.h-fe@nhk.or.jp

The ORCID identification number(s) for the author(s) of this article can be found under https://doi.org/10.1002/admi.202201925.

© 2022 The Authors. Advanced Materials Interfaces published by Wiley-VCH GmbH. This is an open access article under the terms of the Creative Commons Attribution License, which permits use, distribution and reproduction in any medium, provided the original work is properly cited.

DOI: 10.1002/admi.202201925

 © 2022 The Authors. Advanced Materials Interfaces published by Wiley-VCH GmbH

Pictiva EX2007
Samsung v Pictiva
IPR2026-00129

ADVANCED MATERIALS INTERFACES
www.advmatinterfaces.de

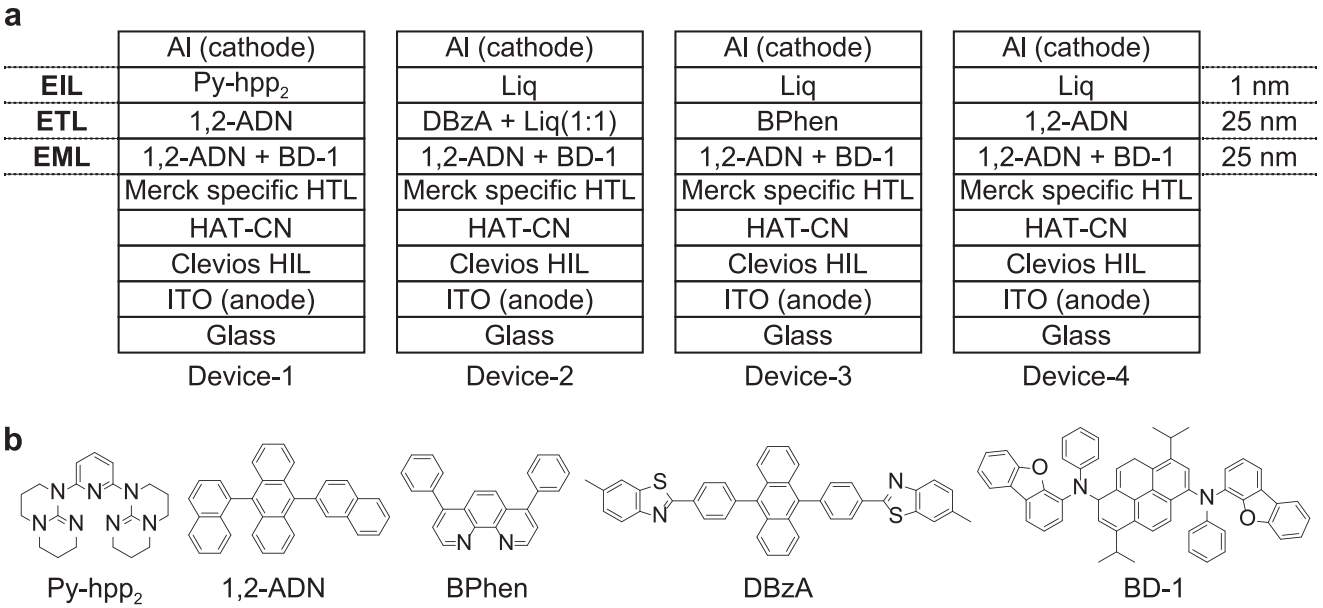

Figure 1. a) Multilayer structure of blue OLEDs. b) Molecular structures of the materials used in the EIL, ETL, and EML.

blue OLEDs is ≈2.0 eV, which is equivalent to the WF near the cathode with Py-hpp$_2$. The energy barrier between the cathode and the EML can be reduced to almost zero by using Py-hpp$_2$. On the other hand, the WFs near the cathode with Li compounds were over 3.0 eV, and a relatively large energy barrier between the cathode and the EML exists when Li compounds are used. We found that the use of Py-hpp$_2$ can optimize the energy levels in blue OLEDs, resulting in the demonstration of a blue OLED with an extremely low operating voltage.

2. Results

2.1. Device Characteristics of Blue OLEDs

The effect of the actual energy diagram in OLEDs on their characteristics was investigated by fabricating and evaluating blue fluorescent OLEDs using four ETL/EIL combinations, as shown in **Figure 1**a,b. The anthracene derivative 9-(1-naphthyl)-10-(2-naphthyl)anthracene (1,2-ADN) was used as the emitting host and N1,N6-*bis*(dibenzo [b,d]furan-4-yl)-3,8-diisopropyl-N1,N6-*bis*(4-isopropylphenyl)-3a1,5-dihydropyrene-1,6-diamine (BD-1) was used as the emitter.[16] The two main reasons why we selected 1,2-ADN as the host are that the use of an anthracene derivative is effective for improving the external quantum efficiency (EQE) of fluorescent OLEDs by utilizing triplet–triplet annihilation[4,24] and that high-performances blue OLEDs fabricated using 1,2-ADN have been reported.[4,25] In previously reported blue OLEDs, compounds with nitrogen-containing heterocycles, such as pyridine, imidazole, and phenanthroline, have been typically used in the ETL, and Li compounds such as (8-quinolinolato)lithium (Liq) have been used in both the EIL and ETL.[16,19,26–30] Among the compounds with nitrogen-containing heterocycles, bathophenanthroline (BPhen) and 9,10-*bis*[4-(6-methylbenzothiazol-2-yl)phenyl]anthracene (DBzA) were used in this study, since they have been reported to be useful for demonstrating fluorescent OLEDs with a low operating voltage.[31] Device-1 and Device-4 were fabricated without the use of compounds with nitrogen-containing heterocycles as the ETL: the emitting host 1,2-ADN was used for both the EML and the ETL. In Device-1 and Device-4, Py-hpp$_2$ and Liq were used as the EIL, respectively. The configurations of Device-2 and Device-3, where the compounds with nitrogen-containing heterocycles and Liq are used as the ETL/EIL, are almost the same as that of previously reported blue OLEDs.[16,19] Liq was used as the EIL in both devices, and DBzA doped with Liq (50 wt%) and BPhen were employed for the ETL Device-2 and Device-3, respectively.

Figure 2a,b shows the current density–voltage and luminance–voltage characteristics of the fabricated blue OLEDs. The operating voltage and other characteristics of the fabricated blue OLEDs are summarized in Table S1, Supporting Information. Clear differences in the operating voltage were observed depending on the ETL and EIL. Device-4 exhibits a high operating voltage despite the use of Liq as the EIL. The operating voltages of Device-2 and Device-3 are much lower than that of Device-4 even though Liq is used as the EIL in all three devices. Although we fabricated a blue OLED with Liq used as the EIL and BPhen doped with Liq used as the ETL, its operating voltage was much higher than that of Device-3 (Figure S1, Supporting Information). Actually, OLEDs fabricated using BPhen doped with Liq as the ETL have rarely been reported. The operating voltage of Device-1 is reduced significantly as compared with that of Device-4 by simply changing the EIL from Liq to Py-hpp$_2$, and its operating voltage is the lowest among the four blue OLEDs. The operating voltages of Device-2 and Device-3 are comparable to those of previously reported blue OLEDs using 1,2-ADN as the host, for which a current density of ≈100 mA cm^{-2} was obtained at an applied voltage of ≈6 V.[25] In contrast, a current density of 100 mA cm^{-2} was obtained at an applied voltage of ≈5 V in Device-1, which is the lowest operating voltage among the blue OLEDs with an anthracene

© 2022 The Authors. Advanced Materials Interfaces published by Wiley-VCH GmbH

Pictiva EX2007
Samsung v Pictiva
IPR2026-00129

21967350, 2023, 19, Downloaded from https://onlinelibrary.wiley.com/doi/10.1002/admi.202201925, Wiley Online Library on [04/10/2024]. See the Terms and Conditions (https://onlinelibrary.wiley.com/terms-and-conditions) on Wiley Online Library for rules of use; OA articles are governed by the applicable Creative Commons License

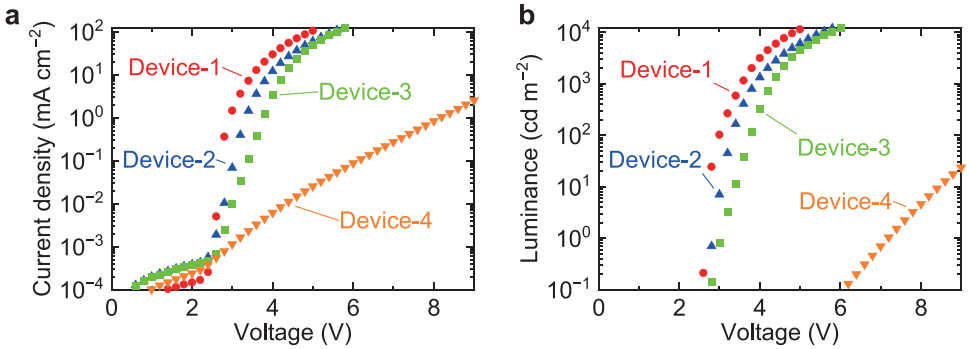

Figure 2. a) Current density–voltage characteristics of blue OLEDs. b) Luminance–voltage characteristics of blue OLEDs.

derivative as the host reported so far.[16,25,27,32] Although the voltage at which the slope of the current density changes is not significantly different between the four devices, clear differences in the increase in current density were observed for different materials used as the ETL and EIL. It is reasonable to assume that the difference in current density at a given applied voltage is caused by the difference in applied voltage required to deliver electrons from the cathode to the EML. The luminance turn-on voltage of Device-4 is much higher than those of the other devices because the luminous efficiency (external quantum efficiency) of Device-4 is much lower than those of the other devices due to the carrier imbalance (Table S1, Supporting Information).

2.2. Analysis of Energy Levels in Blue OLEDs

To understand the observed differences in the operating voltages, we investigated the energy-level alignment between the cathode and the emitting host 1,2-ADN. The actual EA and WF near the cathode were measured by LEIPS and ultraviolet photoelectron spectroscopy (UPS). **Figure 3**a shows the LEIPS

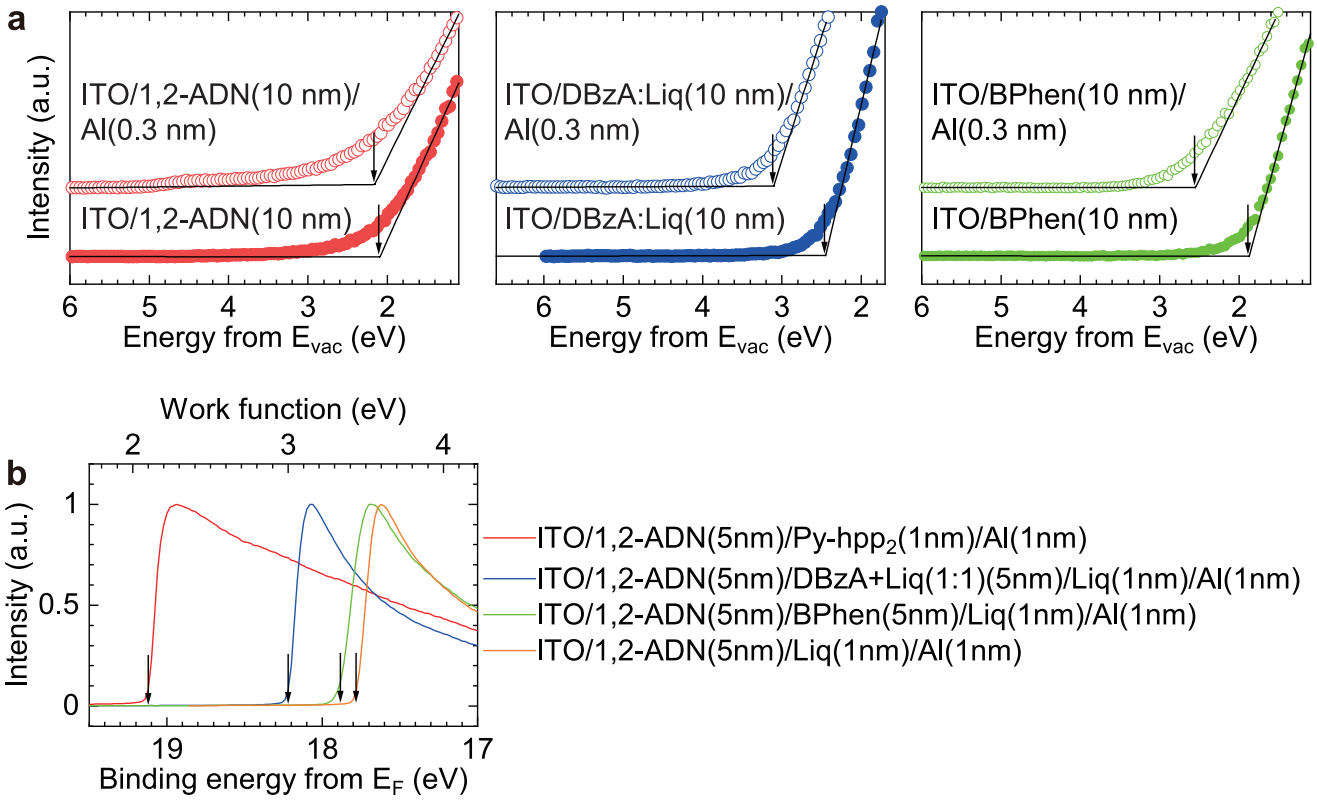

Figure 3. a) LEIPS spectra of Liq-doped DBzA, BPhen, and 1,2-ADN films on ITO (filled symbols) and LEIPS spectra of 0.3-nm-thick Al deposited on each film (open symbols). The electron affinities indicated by arrows were estimated using the "onset of slope" application in ORIGINPRO 2022b software. The horizontal axis is the energy with respect to the vacuum level. b) HeI UPS spectra of each film in secondary regions.

© 2022 The Authors. Advanced Materials Interfaces published by Wiley-VCH GmbH

Pictiva EX2007
Samsung v Pictiva
IPR2026-00129

21967350, 2023, 19, Downloaded from https://onlinelibrary.wiley.com/doi/10.1002/admi.202201925, Wiley Online Library on [04/10/2024]. See the Terms and Conditions (https://onlinelibrary.wiley.com/terms-and-conditions) on Wiley Online Library for rules of use; OA articles are governed by the applicable Creative Commons License

ADVANCED MATERIALS INTERFACES
www.advmatinterfaces.de

spectra of the three materials used as the ETL, where the filled symbols represent the LEIPS spectra of only the ETL and the open symbols represent the LEIPS spectra of 0.3-nm-thick Al deposited on the ETL. We see from the filled symbols that the actual EAs of 1,2-ADN, Liq-doped DBzA, and BPhen are 2.10, 2.45, and 1.87 eV, respectively. Although the EA of anthracene derivatives suitable for blue OLEDs has been estimated to be over 2.7 eV from the IP and the absorption spectrum,[25,27] the actual EA of 1,2-ADN was found to be much smaller by LEIPS measurement. It is also important to measure the EA of the ETL with 0.3-nm-thick Al (Figure 3a, open symbols), since the EA around the cathode can change owing to the coordination reaction.[33] Yoshida et al. have clarified by LEIPS that the EA of 2,9-dimethyl-4,7-diphenyl-1,10-phenanthroline (BCP) can change from 1.9 to 2.7 eV through the coordination reaction with Ag, and this change in the EA plays a key role in electron injection/collection to the Ag cathode. In addition, we previously reported that the coordination reaction between a pyridine derivative and Al reduces the electron injection barrier between the cathode and the ETL.[23] We see from the open symbols in Figure 3a that the EA of Liq-doped DBzA and BPhen increases by ≈0.7 eV owing to the deposition of Al. It is reasonable to assume that the change in the EA is caused by the coordination reaction between Al and nitrogen in BPhen/DBzA. It has been recently reported that the coordination reaction induces a change in the EA, as mentioned above, and we have newly observed changes in the EA for two compounds with nitrogen-containing heterocycles. It is natural that the EA of 1,2-ADN is almost unchanged by the deposition of Al since 1,2-ADN is an aromatic hydrocarbon. In past reports on blue OLEDs, device characteristics have been discussed by using inaccurate energy diagrams, where the EA of the host is larger than the actual EA, and the change in the EA near the cathode due to the coordination reaction is not considered.[17,19,25,31] Figure 3b shows the UPS spectra of the 1-nm-thick Al deposited on glass/indium tin oxide (ITO)/host/ETL/EIL thin films. The secondary cutoff of the spectrum, which is indicated by an arrow, corresponds to the WF at the cathode/organic layer interface of each OLED. The WFs near the cathodes of Device-1, Device-2, Device-3, and Device-4 were observed to be 2.10, 3.00, 3.33, and 3.43 eV, respectively. The insertion of Py-hpp$_2$ between 1,2-ADN and Al reduced the WF of Al to ≈2 eV, consistent with a previous report.[23] WFs smaller than 3.3 eV were obtained in Device-2 and Device-3, where the EIL/ETL configuration is a combination of Liq and compounds with nitrogen-containing heterocycles. It is reasonable to suppose that the observed relatively low WF is caused by the low charge neutrality level of Liq and the coordination reaction.[33,34] The results shown in Figure 3 enable us to determine the accurate energy level between the cathode and the EML.

3. Discussion

The operating voltages of blue OLEDs were successfully correlated with the actual energy-level alignment around the cathode in each OLED estimated by LEIPS and UPS. The energy-level alignment between the cathode and the EML in each OLED is described in **Figures 4**a–d. As shown in Figure 4, there are two main energy barriers in the delivery of electrons from the cathode to the emitting host (1,2-ADN): one is the energy barrier between the cathode and the ETL, and the other is the energy barrier between the ETL and 1,2-ADN. The energy barrier between the cathode and the ETL has been reported to have a significant effect on the operating voltage,[23] and the energy barrier between the ETL and the EML has also been reported to affect the operating voltage.[35] In Device-1 with Py-hpp$_2$ used as the EIL, which exhibited the lowest operating voltage, the energy barrier between the cathode and the ETL is zero, and the energy barrier between the ETL and the EML is also zero because both the ETL and the host are 1,2-ADN. It is important to note that the operating voltage required to reach 24 cd m^{-2} is 2.8 V for Device-1, which is smaller than the actual band gap of 1,2-ADN (3.7 eV), as shown in Figure 2b (Figure S2, Supporting Information). There have been several reports on OLEDs that operate below the band gap, for which n-doped ETLs are used.[15,36] Therefore, charge recombination at an operating voltage smaller than the band gap of the EML is expected to be possible if electrons can be delivered efficiently from the cathode to the EML. In Device-2, the energy barrier between the cathode and the ETL is zero owing to the coordination reaction of DBzA with Al, whereas there is an energy barrier of 0.35 eV between the ETL and the EML as shown in Figure 4b. In the case of Device-3, the energy barrier between the cathode and the ETL is significantly decreased by the coordination reaction between BPhen and Al; nevertheless, there is

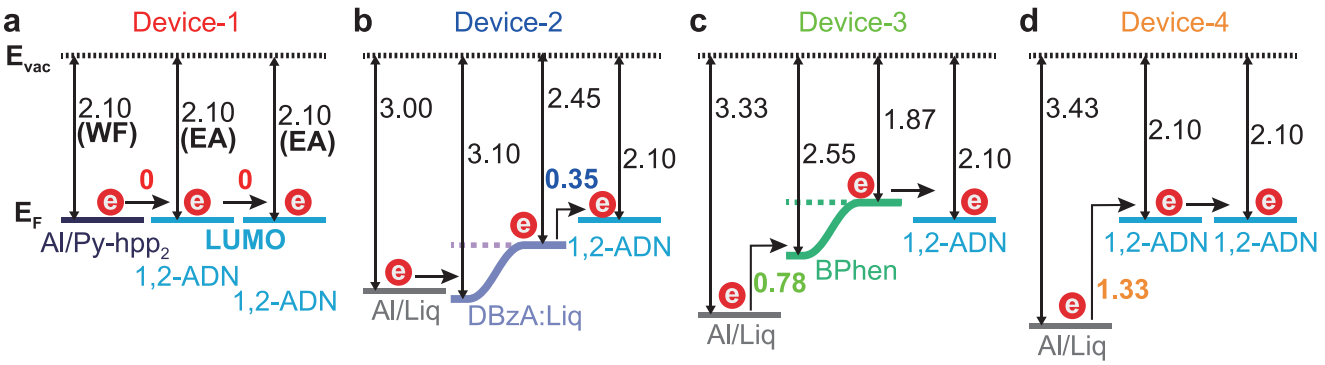

Figure 4. Summary of energy diagrams from the cathode to the emitting layer of a) Device-1, b) Device-2, c) Device-3, and d) Device-4 estimated from LEIPS and UPS spectra, where E_F and E_{vac} represent the Fermi and vacuum levels, respectively.

© 2022 The Authors. Advanced Materials Interfaces published by Wiley-VCH GmbH

Pictiva EX2007
Samsung v Pictiva
IPR2026-00129

21967350, 2023, 19, Downloaded from https://onlinelibrary.wiley.com/doi/10.1002/admi.202201925, Wiley Online Library on [04/10/2024]. See the Terms and Conditions (https://onlinelibrary.wiley.com/terms-and-conditions) on Wiley Online Library for rules of use; OA articles are governed by the applicable Creative Commons License

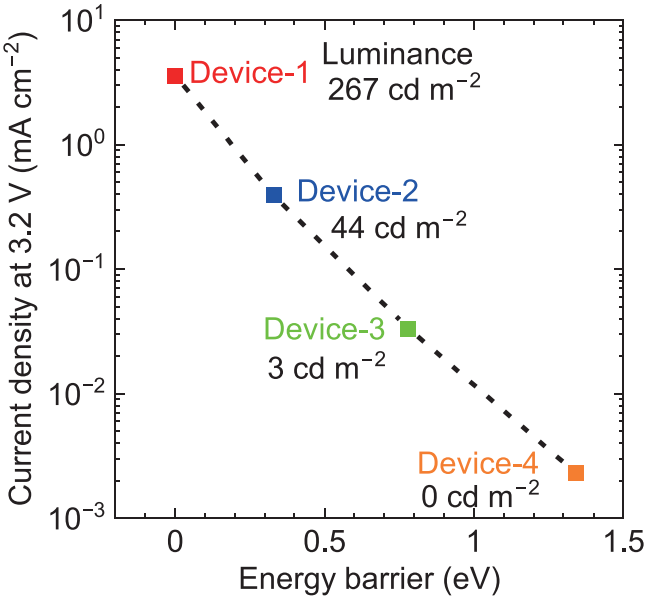

Figure 5. Correlation between the current density and the energy barrier between the cathode and the EML for the four OLEDs. The values in the panel indicate the luminance at an applied voltage of 3.2 V for each OLED.

still an energy barrier of 0.78 eV. There is a large energy barrier of 1.33 eV between the cathode (EIL) and the ETL in Device-4 since there is no coordination reaction between 1,2-ADN and Al. The correlation between the energy barrier in delivering electrons from the cathode to the EML and the current density of OLEDs is summarized in **Figure 5**. The vertical axis shows the current density of each OLED at an applied voltage of 3.2 V, and the horizontal axis shows the energy barrier between the cathode and the EML. We selected the applied voltage of 3.2 V because visible luminance (over 1 cd m^{-2}) was observed in three OLEDs (Device-1, Device-2, and Device-3) at this voltage. Since there is no direct correlation between the energy barrier and the luminance of the four OLEDs with different EQEs, their luminances are included as reference values. A large energy barrier in Device-4 causes an imbalance between holes and electrons. As a result, the EQE of Device-4 is greatly reduced, and the current density required to obtain a luminance of 1 cd m^{-2} becomes extremely larger than those of other devices (Figure 2b, Table S1, Supporting Information). As can be seen from Figure 5, there is a strong correlation between the energy barrier and the current density at an applied voltage of 3.2 V for each OLED. A similar tendency was observed at different applied voltages (Figure S3, Supporting Information). Thus, we can conclude that the clear differences in the increase in current density shown in Figure 2a are caused by the difference in the energy barrier between the cathode and the EML. This correlation could only be observed by precisely examining the energy-level alignment between the cathode and the EML using LEIPS and UPS. It is reasonable to assume that the effect of the electron mobility of the material used as the ETL on the operating voltage is small since the ETL thickness is only 25 nm.[23]

The reason why the operating voltage of Device-1 is the lowest among blue OLEDs fabricated using an anthracene derivative as the host reported so far is that this is the only blue OLED for which the energy barrier between the cathode and the EML is almost zero. In the previously reported blue OLEDs, where Li compounds and compounds with nitrogen-containing heterocycles were used as the EIL/ETL, a small energy barrier of lower than 1 eV is expected to exist, as with Device-2 and Device-3. On the basis of the energy-level alignment estimated by LEIPS and UPS, a relatively large energy barrier of ≈1 eV exists between the cathode and the EML, since the WF of the cathode with Li compounds is ≈3 eV and the EA of the material used in the blue EML is ≈2 eV. The change in the EA of compounds with nitrogen-containing heterocycles used as the ETL, which is caused by the coordination reaction, can contribute to reducing the energy barrier; however, it is not easy to make the energy barrier zero. Since the low-WF electrodes realized by using Py-hpp$_2$ can remove this energy barrier, the use of Py-hpp$_2$ is expected to contribute significantly to improving the performances of blue OLEDs.

4. Conclusion

We conclude that the energy barrier between the cathode and the EML is a key factor in determining the operating voltages of blue OLEDs. This could only be clarified by associating the differences in the ETL/EIL-dependent characteristics of blue OLEDs with the exact energy levels revealed by LEIPS and UPS. For a blue OLED with an extremely low operating voltage, the WF of the cathode can be aligned with the EA of the emitting host by using Py-hpp$_2$, and the energy barrier is zero. On the other hand, we find that it remains difficult to remove the energy barrier completely in typical blue OLEDs with Li compounds and compounds with nitrogen-containing heterocycles used as the EIL/ETL. Therefore, this energy barrier may have been a bottleneck in improving the performances of blue OLEDs. Our discovery that low-WF electrodes are suitable for lowering the operating voltages of blue OLEDs is expected to markedly improve the performances of blue OLEDs.

5. Experimental Section

Fabrication of Blue OLEDs: Blue fluorescent OLEDs were fabricated on glass substrates coated with a 70-nm-thick ITO layer. Prior to the fabrication of the organic layers, the substrate was cleaned using ultrapure water and organic solvents and by UV–ozone treatment. After the UV–ozone treatment, Clevios HIL 1.3 N (supplied by Heraeus Holding GmbH) was spun onto the substrate to form a 10-nm-thick layer. Clevios HIL 1.3 N was effective for not only injecting holes from the ITO, but also reducing the possibility of electrical shorts within the device. The other organic layers were sequentially deposited onto the substrate without breaking the vacuum with a pressure of ≈10^{-5} Pa. The film structure of the blue fluorescent OLEDs was ITO (70 nm)/Clevios HIL 1.3 N (10 nm)/HAT-CN (5 nm)/Merck specific HTL (30 nm)/1,2-ADN:BD-1 (5 wt%, 25 nm)/ETL (25 nm), where HAT-CN was 1,4,5,8,9,11-hexaazatriphenylenehexacarbonitrile. After the ETL was formed, the EIL was deposited. In the OLEDs, 1-nm-thick Liq and Py-hpp$_2$ were used as the EILs. After the formation of each EIL, a 100-nm-thick Al layer was deposited as the cathode. The devices were encapsulated using a UV-epoxy resin and a glass cover in nitrogen atmosphere after cathode formation.

© 2022 The Authors. Advanced Materials Interfaces published by Wiley-VCH GmbH

Pictiva EX2007
Samsung v Pictiva
IPR2026-00129

21967350, 2023, 19, Downloaded from https://onlinelibrary.wiley.com/doi/10.1002/admi.202201925, Wiley Online Library on [04/10/2024]. See the Terms and Conditions (https://onlinelibrary.wiley.com/terms-and-conditions) on Wiley Online Library for rules of use; OA articles are governed by the applicable Creative Commons License

Device Characterization: The luminance was measured using a Minolta LS-110 luminance meter. A Keithley 2400 Digital SourceMeter and a desktop computer were used to operate the devices.

UPS Measurement: Glass substrates coated with a 150-nm-thick ITO layer were cleaned with ultrapure water and organic solvents. After UV–ozone treatment, organic thin films and/or metals were deposited using a vacuum evaporation system. UPS spectra of the samples were measured using a CHA analyzer with a 128-channel detector; the excitation source was a HeI (21.22 eV) discharge lamp. A bias of −8.0 V was applied to each sample to separate the sample and the secondary edge for the analyzer.

LEIPS Measurement: LEIPS spectra of organic thin films and/or metals deposited on glass/ITO using a vacuum evaporation system were measured using an LEIPS measurement system (ALS Technology Co., Ltd.). ITO substrates were used for the LEIPS measurement because the spectral features can be observed clearly due to the low background signal. No discernible dependence on the sample current or photon energy was observed, confirming that the LEIPS spectra were free from sample charging. A bandpass filter with a center wavelength of 260 nm was used. The EA was obtained by the standard procedure for determining the ionization energy by UPS. The onset of the LEIPS spectrum was determined as the intersection of the straight line fitted to the onset region of the spectrum and the baseline.

Supporting Information

Supporting Information is available from the Wiley Online Library or from the author.

Acknowledgements

The authors thank Heraeus Holding GmbH for supplying Clevios HIL 1.3 N.

Conflict of Interest

The authors declare no conflict of interest.

Data Availability Statement

The data that support the findings of this study are available from the corresponding author upon reasonable request.

Keywords

electron affinity, energy-level alignment, low work function, low-energy inverse photoemission spectroscopy, organic light-emitting diodes

Received: August 30, 2022
Revised: October 20, 2022
Published online: December 4, 2022

[1] G. Hong, X. Gan, C. Leonhardt, Z. Zhang, J. Seibert, J. M. Busch, S. Bräse, *Adv. Mater.* **2021**, *33*, 2005630.
[2] C.-Y. Chan, M. Tanaka, Y.-T. Lee, Y.-W. Wong, H. Nakanotani, T. Hatakeyama, C. Adachi, *Nat. Photonics* **2021**, *15*, 203.
[3] H. Uoyama, K. Goushi, K. Shizu, H. Nomura, C. Adachi, *Nature* **2012**, *492*, 234.
[4] D. Y. Kondakov, T. D. Pawlik, T. K. Hatwar, J. P. Spindler, *J. Appl. Phys.* **2009**, *106*, 124510.
[5] C. Adachi, M. A. Baldo, M. E. Thompson, S. R. Forrest, *J. Appl. Phys.* **2001**, *90*, 5048.
[6] M. A. Baldo, D. F. O'Brien, Y. You, A. Shoustikov, S. Sibley, M. E. Thompson, S. R. Forrest, *Nature* **1998**, *395*, 151.
[7] J. Kido, M. Kimura, K. Nagai, *Science* **1995**, *267*, 1332.
[8] C. W. Tang, S. A. VanSlyke, *Appl. Phys. Lett.* **1987**, *51*, 913.
[9] Z. Xu, B. Z. Tang, Y. Wang, D. Ma, *J. Mater. Chem. C* **2020**, *8*, 2614.
[10] D. Wang, C. Cheng, T. Tsuboi, Q. Zhang, *CCS Chem.* **2020**, *2*, 1278.
[11] J.-H. Lee, C.-H. Chen, P.-H. Lee, H.-Y. Lin, M. Leung, T.-L. Chiu, C.-F. Lin, *J. Mater. Chem. C* **2019**, *7*, 5874.
[12] K. Walzer, B. Maennig, M. Pfeiffer, K. Leo, *Chem. Rev.* **2007**, *107*, 1233.
[13] T. Oyamada, C. Maeda, H. Sasabe, C. Adachi, *Jpn. J. Appl. Phys.* **2003**, *42*, L1535.
[14] L. S. Hung, C. W. Tang, M. G. Mason, *Appl. Phys. Lett.* **1997**, *70*, 152.
[15] Y. Deng, C. Murawski, C. Keum, K. Yoshida, I. D. W. Samuel, M. C. Gather, *Adv. Opt. Mater.* **2020**, *8*, 1901721.
[16] T. Sato, T. Miyamae, H. Ohata, T. Tsutsui, *Org. Electron.* **2019**, *74*, 118.
[17] S. H. Choi, S. J. Lee, K. Y. Lee, H. S. Yang, K. Han, K. H. Kim, S. D. Kim, H. D. Bae, Y. H. Tak, *Jpn. J. Appl. Phys.* **2009**, *48*, 062101.
[18] S.-H. Eom, Y. Zheng, E. Wrzesniewski, J. Lee, N. Chopra, F. So, J. Xue, *Org. Electron.* **2009**, *10*, 686.
[19] B. Y. Kim, S. J. Lee, J.-R. Koo, S. E. Lee, K. H. Lee, S. S. Yoon, Y. K. Kim, *Displays* **2013**, *34*, 396.
[20] H. Yoshida, K. Yoshizaki, *Org. Electron.* **2015**, *20*, 24.
[21] H. Yoshida, *J. Electron Spectrosc. Relat. Phenom.* **2015**, *204*, 116.
[22] R. J. Schwamm, R. Vianello, A. Maršavelski, M. Á. García, R. M. Claramunt, I. Alkorta, J. Saame, I. Leito, C. M. Fitchett, A. J. Edwards, M. P. Coles, *J. Org. Chem.* **2016**, *81*, 7612.
[23] T. Sasaki, M. Hasegawa, K. Inagaki, H. Ito, K. Suzuki, T. Oono, K. Morii, T. Shimizu, H. Fukagawa, *Nat. Commun.* **2021**, *12*, 2706.
[24] H. Fukagawa, T. Shimizu, N. Ohbe, S. Tokito, K. Tokumaru, H. Fujikake, *Org. Electron.* **2012**, *13*, 1197.
[25] Z. Liu, X. Li, Y. Lu, C. Zhang, Y. Zhang, T. Huang, D. Zhang, L. Duan, *Nat. Commun.* **2022**, *13*, 1215.
[26] J. U. Kim, I. S. Park, C.-Y. Chan, M. Tanaka, Y. Tsuchiya, H. Nakanotani, C. Adachi, *Nat. Commun.* **2020**, *11*, 1765.
[27] H. Lim, H. J. Cheon, G. S. Lee, M. Kim, Y.-H. Kim, J.-J. Kim, *ACS Appl. Mater. Interfaces* **2019**, *11*, 48121.
[28] X. Li, J. Zhang, Z. Zhao, L. Wang, H. Yang, Q. Chang, N. Jiang, Z. Liu, Z. Bian, W. Liu, Z. Lu, C. Huang, *Adv. Mater.* **2018**, *30*, 1705005.
[29] S. Hirata, Y. Sakai, K. Masui, H. Tanaka, S. Y. Lee, H. Nomura, N. Nakamura, M. Yasumatsu, H. Nakanotani, Q. Zhang, K. Shizu, H. Miyazaki, C. Adachi, *Nat. Mater.* **2015**, *14*, 330.
[30] S.-J. Su, Y. Takahashi, T. Chiba, T. Takeda, J. Kido, *Adv. Funct. Mater.* **2009**, *19*, 1260.
[31] K. Okumoto, H. Kanno, Y. Hamaa, H. Takahashi, K. Shibata, *Appl. Phys. Lett.* **2006**, *89*, 063504.
[32] J. Park, K. J. Kim, J. Lim, T. Kim, J. Y. Lee, *Adv. Mater.* **2022**, *34*, 2108581.
[33] H. Yoshida, *J. Phys. Chem. C* **2015**, *119*, 24459.
[34] S. Park, Y. Yi, S. W. Cho, H. Lee, *Chem. Phys. Lett.* **2016**, *652*, 102.
[35] R. A. K. Yadav, D. K. Dubey, S.-Z. Chen, T.-W. Liang, J.-H. Jou, *Sci. Rep.* **2020**, *10*, 9915.
[36] H. Sasabe, H. Nakanishi, Y. Watanabe, S. Yano, M. Hirasawa, Y.-J. Pu, J. Kido, *Adv. Funct. Mater.* **2013**, *23*, 5550.

© 2022 The Authors. Advanced Materials Interfaces published by Wiley-VCH GmbH

Pictiva EX2007
Samsung v Pictiva
IPR2026-00129

21967350, 2023, 19, Downloaded from https://onlinelibrary.wiley.com/doi/10.1002/admi.202201925, Wiley Online Library on [04/10/2024]. See the Terms and Conditions (https://onlinelibrary.wiley.com/terms-and-conditions) on Wiley Online Library for rules of use; OA articles are governed by the applicable Creative Commons License